# Magnetization process and magnetoimpedance in (110)[001] FeSi 3%

M. Carara, A. Gündel, M. N. Baibich, and R. L. Sommer

Citation: Journal of Applied Physics **84**, 3792 (1998); doi: 10.1063/1.368557
View online: http://dx.doi.org/10.1063/1.368557
View Table of Contents: http://scitation.aip.org/content/aip/journal/jap/84/7?ver=pdfcov
Published by the AIP Publishing

# Magnetization process and magnetoimpedance in (110)[001]$FeSi_{3\%}$

M. Carara[a)]
*Instituto de Física, Universidade Federal do Rio Grande do Sul, 91501-970 Porto Alegre, RS, Brazil*

A. Gündel
*Departamento de Física, Universidade Federal de Santa Maria, 97105-900 Santa Maria, RS, Brazil*

M. N. Baibich
*Instituto de Física, Universidade Federal do Rio Grande do Sul, 91501-970 Porto Alegre, RS, Brazil*

R. L. Sommer[b)]
*Departamento de Física, Universidade Federal de Santa Maria, 97105-900 Santa Maria, RS, Brazil*

(Received 5 December 1997; accepted for publication 2 July 1998)

The present article investigates the relation between magnetoimpedance (MI) and the evolution of the magnetic domain structure along the magnetization curves of commercial $FeSi_{3\%}$ sheets cut at different angles with respect to the easy magnetization axis [001]. The role of the magnetocrystalline anisotropy on MI is studied and the correlation between the basic features of the MI vs $H$ and magnetization ($M$) vs $H$ curves is established. From data obtained at appropriate frequency ranges, the frequency dependence of the effective transverse differential permeability is obtained. The frequency and field spectra of the impedance allow the identification of the rotation of the magnetization as the main contribution of the magnetization processes to the MI effects in the studied samples. © *1998 American Institute of Physics.* [S0021-8979(98)04419-3]

## I. INTRODUCTION

The dependence on frequency, of the impedance of a conductor carrying an alternating current has been a known issue for a long time.[1,2] Recently, this dependence attracted a great deal of attention and has been widely studied in soft magnetic conductors in view of its potential application in magnetic-field sensors.[3–5] The underlying mechanism involved is the skin effect, whose main parameter is the skin-depth $\delta_m = \sqrt{\rho/\pi\mu_{\text{eff}}f}$ and the dependence of the effective transverse permeability $\mu_{\text{eff}}(H, I_{\text{ac}}, f)$, on the external dc field ($H$), as well as on the frequency ($f$) and amplitude of the ac probe current ($I_{\text{ac}}$).[6,7] So far, these magnetoimpedance effects (MI) have been studied in detail in soft amorphous magnetic materials, shaped as wires,[3,4,6] ribbons,[5,8] or films,[9–11] with both large[10] and nearly zero[12,13] magnetostriction. These materials exhibit high permeability and low losses at high frequencies, desirable characteristics in order to exhibit large MI ratios. As the main anisotropy sources in amorphous materials are the induced and magnetoelastic anisotropies, the effect of these particular anisotropies on the MI have been extensively investigated.[8,13–15]

Recently, we reported a large MI effect in grain-oriented highly anisotropic $FeSi_{3\%}$,[16] which exhibited very interesting MI vs $H$ curves for different angles between the [001] axis and the applied field direction. In this work, a more complete analysis of the MI effect on (110)[001]$FeSi_{3\%}$ is made and the correlation between the MI and the magnetic domain structure evolution along the hysteresis curve for each sample is established.

## II. EXPERIMENT

The samples were spark cut from an ANSI M5 commercial sheet (produced by Nippon Steel) in rectangular shapes (10.0 mm long, 1.0 mm wide, and 0.3 mm thick) at angles $\theta$ between the [001] easy axis and the sample's length, ranging from 0° to 90° (10° steps). The samples are textured, with large grains (diameter ~5 mm), in such a way that each one has just a few grain boundaries. The magnetizing field ($H$) was provided by a long solenoid and applied always parallel to the $I_{\text{ac}}$ and to the sample's length.

MI measurements were carried out using a standard four-probe ac method. For frequencies up to 100 kHz, a dual phase lock-in amplifier was used to detect the voltage proportional to the impedance $Z^* = V^*_{\text{lock-in}}/I_{\text{ac}}$. For the frequency range $100\ \text{kHz} \leqslant f \leqslant 20\ \text{MHz}$, the absolute value of the complex voltage was measured by means of a rf differential amplifier followed by a diode-based detector. Electric contacts were spark welded, giving ultralow contact resistance and avoiding possible effects from stray capacitances at high frequencies. The voltage leads were nearly 7 mm apart for all samples.

Coaxial cables for the probe current and signal detection were carefully 50 Ω matched and made as short as possible in order to reduce eventual cable effects. As the sample resistance and its variation under $H$ and $f$ are small (~30 mΩ) compared to the cable matching resistance, the probe current amplitude was determined as the voltage drop across the matching plus sample resistances divided by the value of the matching one.

The magnetization curves were obtained by integration of the voltage signal sensed by a coil wound on the same

[a)]On leave from Departamento de Física, UFSM.
[b)]Corresponding author: Electronic mail: sommer@ccne.ufsm.br

 

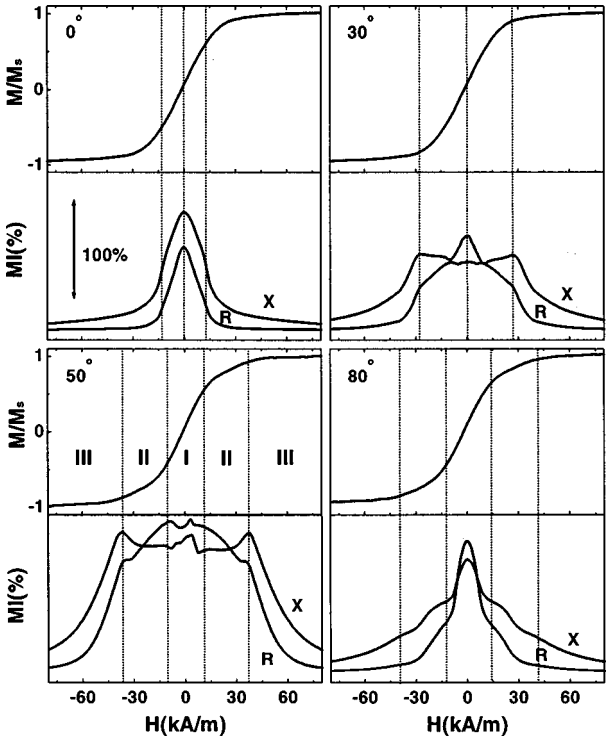


FIG. 1. Magnetization curves corresponding to the real ($R$) and imaginary ($X$) components of the MI field spectra of some samples taken at $f=100$ kHz and $I_{ac}=4$ mA$_{rms}$.

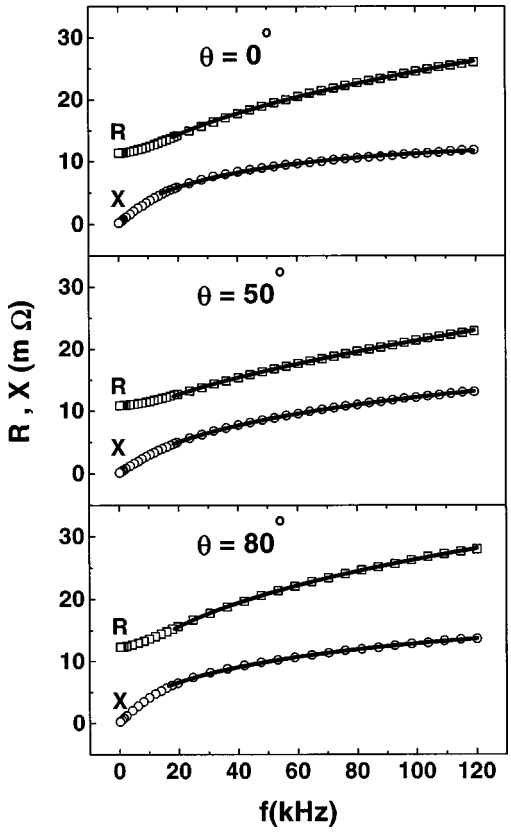


FIG. 2. Representative frequency spectra of MI for the set of studied samples. All measurements were taken at zero applied field.

samples used for the MI measurement. The field sweep was quasistatic and all measurements were made at room temperature.

## III. RESULTS

The MI vs $H$ curves for $\theta=0°$, 30°, 50°, and 80° samples are shown in Fig. 1. The curves were obtained with probe current amplitude $I_{ac}=4$ mA$_{rms}$ and frequency 100 kHz. The results are presented as $\Delta R/R_S=100[R(H)-R_S]/R_S$ and $\Delta X/R_S=100[X(H)-X_S]/R_S$, where $R$ and $X$ are the real and imaginary components of the impedance, respectively, and $R_S$ and $X_S$ are their saturation values. By expressing MI in this way, changes in both components of the impedance can be directly compared. In the same figure, the corresponding magnetization curves are shown. The connections between the main features of the magnetization and MI vs $H$ curves are indicated by dashed vertical lines. As it is well known, (110)[001]FeSi$_{3\%}$ is a soft magnetic material largely used in power transformers and machines. Thus, at first sight, the saturation field appears to be high (~120 kA/m) and, as a consequence, the MI sensitivity seems to be very low. By superimposing both, MI vs $H$ and $M/M_S$ vs $H$ curves, it becomes clear that the high saturation fields are mainly due to the high demagnetization factors of the samples. These magnetization curves are typical of samples cut from a material with (110)[001] texture and exhibiting high anisotropy constants like FeSi$_{3\%}$ [$K_1\approx 2.8\times 10^4$ J/m$^3$ and $K_2\approx 10^4$ J/m$^3$ (Ref. 17)].

It can be seen from Fig. 1 that there is an evolution of both, the amplitude and shape of the MI vs $H$ curves as the angle $\theta$ is changed, resulting from the magnetocrystalline anisotropy effect on the transverse effective permeability. At the extreme angles 0° and 90° (not shown), the MI vs $H$ curves are smooth, with a single peak centered at $H=0$. For the $20°\leqslant\theta\leqslant 70°$ samples, represented by the curves for $\theta=30°$ and 50° in Fig. 1, lateral peaks do appear. The field value where these features are observed coincide with the appearance of additional knees on the magnetization curves, as indicated by the vertical dashed lines in Fig. 1.

In Fig. 2, the frequency dependence of the impedance measured at $H=0$, for the $\theta=0$, 50° and 80° samples is shown. From Fig. 2, the general behavior described by Panina *et al.*[9] for an amorphous wire can be seen, i.e., at the low-frequency range ($f<10$ kHz), $X(f)$ exhibits a linear increase with $f$, while $R(f)$ is roughly constant (magnetoinductive effect). For the high-frequency range ($15\text{ kHz}\leqslant f\leqslant 100$ kHz), both components present a $f^{1/2}$ response, corroborated by the fitted lines shown in Fig. 2. From the $f^{1/2}$ response, it can be concluded that the effective transverse permeability ($\mu_{eff}$) is constant while this dependence holds.

The general features of the field and frequency behavior do not change under different ac measuring current amplitudes. Measurements made with current amplitudes in the range 0.05–35 mA (not shown) resulted in roughly constant values of $R(f)$ and $X(f)$ for a given value of the external field $H$.

In Fig. 3, MI vs $H$ curves taken at frequencies of 1, 10, and 100 kHz for the $\theta=0°$, 50°, and 80° samples are shown. The $\theta=0°$ sample shows MI vs $H$ curve with a single peak,

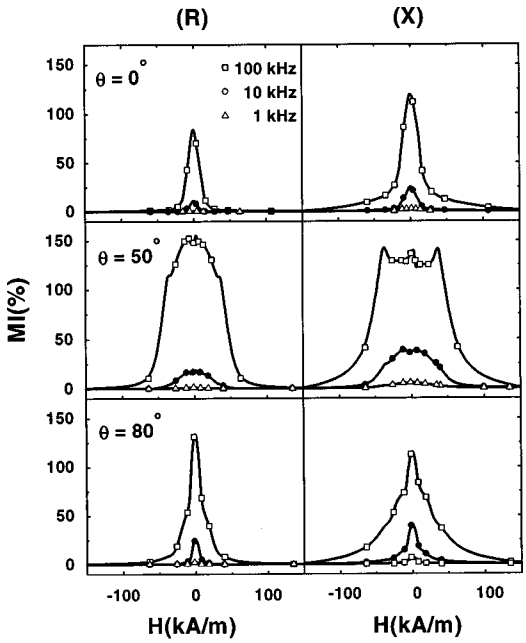


FIG. 3. Real and imaginary components of MI for selected samples at 1, 10, and 100 kHz.

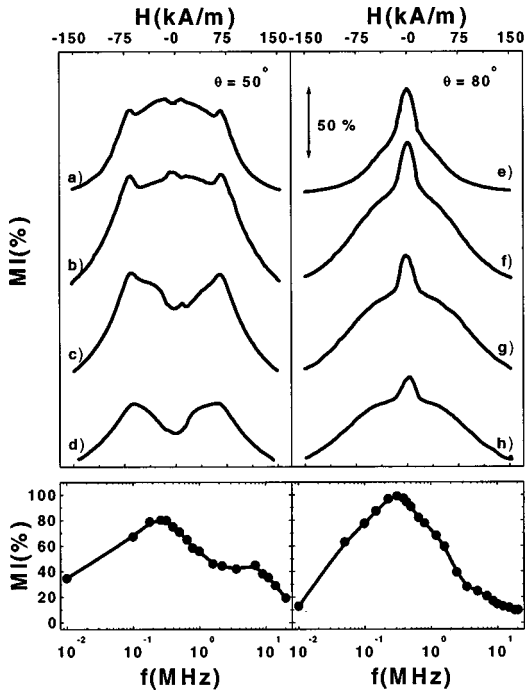


FIG. 4. High-frequency MI field spectra for the $\theta$=50° and 80° samples. (a)–(d) stands for frequencies of 0.1, 0.32, 2.2, and 20 MHz, respectively, while (e)–(h) stands for the frequencies of 0.1, 0.31, 0.65, and 1.6 MHz, respectively. The bottom layer corresponds to the percent changes in MI as a function of frequency.

without evolution of a secondary structure as the measuring frequency is increased. For the $\theta$=50° sample, while the $R$ vs $H$ curves present no evolution as $f$ is increased, the $X$ vs $H$ curves are strongly affected. For the low-frequency regime, there is a central valley on $X(H,f)$ while for high frequencies, central and lateral peaks are observed. The $\theta$=80° sample exhibits field and frequency dependencies similar to the $\theta$=50° sample, except for the central valley in the lower-frequency range. The general field and frequency dependence of the $\theta$=70°–90° samples are similar to the $\theta$=0° sample, while for $20° \leqslant \theta \leqslant 60°$, the samples present the same general trend as the $\theta$=50° sample.

The MI vs $H$ curves obtained for frequencies between 100 kHz and 20 MHz are shown in Fig. 4 for the $\theta$=50° and $\theta$=80° samples. In Fig. 4, MI is expressed as $100[Z(H)-Z_s]/Z_s$, where $Z(H)$ is the impedance at field $H$, and $Z_s$ is its saturation value. The main feature of MI vs $H$ curves for these higher frequencies is the increase of the lateral peaks while the central peaks decrease, in a way consistent with the high-frequency behavior of the MI, as pointed out by Panina and co-workers.[9] The lower panel in the same figure displays the frequency dependence of the MI amplitude, which exhibits a maximum for frequencies around 300 kHz.

## IV. DISCUSSION

As seen from Fig. 1, the details of the MI vs $H$ curves observed in this work can be associated with the magnetization processes of the (110)[001]$FeSi_{3\%}$ samples. In order to analyze this connection, it is worth remembering that this particular material is characterized by an average spread of the angle between the (110) crystalline plane and the sample's surface (tilt angle), of about 4°. This misalignment gives rise to free-magnetic poles at the sample surfaces, which lead to the formation of a closure domain structure, known as the ''lancet domain structure.'' The evolution of this structure has been extensively studied due to its connection to power losses in $FeSi_{3\%}$.[18–22] Each ''lancet domain'' can, in fact, be divided in three parts, as shown in Fig. 5, where a schematic drawing of this structure for a sample in the demagnetized state is shown. Two of them are located at the opposite (top and bottom surfaces) of the sheet. They have the shape of a pyramid whose triangular basis is in the (110) plane. The third part connects the first two through magnetization vectors aligned along the [010] or [100] axis, which are also magnetic easy directions.[17,18]

### A. Domain structure evolution during magnetization

The domain structure of the (110)[001]$FeSi_{3\%}$ samples along the magnetization curves must be consistent with a condition of the minimum of the magnetic free energy, whose main contributions are the magnetostatic, magnetocrystalline, and magnetoelastic energies.[17,18] In order to minimize these energies, the domain structure is modified accordingly when an external magnetic field is applied.

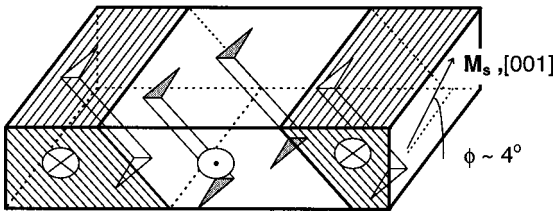


FIG. 5. Domain structure of the (110)[001]$FeSi_{3\%}$ with a tilt angle of 4° [after Imamura and Sasaki (Ref. 19)].

Thus, the volume of the sample is divided into two kinds of domains: the main striped domains with magnetizations along the [001] axis (volume fraction $\Omega_1$), and the already mentioned lancet domains (volume fraction $\Omega_2$). Eventually, the lancet domains coalesce into bulk longitudinal and surface band domains. Associated with this coalescence, a maximum in $\Omega_2$ appears at intermediate levels of the magnetization process,[18–21] which in turn can be associated with some features in $M$ vs $H$ curves, as seen on the magnetization curves of Fig. 1. Besides domain structure observation by Kerr effect,[21] this peak in $\Omega_2$ is detected through measurements of permeability,[18] Barkhausen noise,[20] and magnetostriction curves.[22] In this work, such evolution was detected through MI measurements.

In order to compare the evolution of the domain structure, qualitatively obtained from the magnetization curves presented in the Fig. 1 to the MI vs $H$ curves, the magnetization stages of a typical $FeSi_{3\%}$ sample are described in the steps below (the $\theta=50°$ sample will be taken as a reference without any lack of generality). Starting from the demagnetized state, the magnetization process will take place through:[18–22]

(i) The main striped domains (with a favorable orientation with respect to the external field) grow at the expenses of less favorable ones. During this process, there is no change in volume fractions $\Omega_1$ and $\Omega_2$. This process occurs at the center of region I shown in the magnetization curve for the $\theta=50°$ sample.

(ii) Some lancet domains broaden up while the 180° domain-wall (DW) motion of the main domains is still taking place. This process occurs at the border of region I.

(iii) Some lancets elongate and possibly coalesce with other lancets, eventually forming longitudinal (band) domains. There is a sudden increase on the volume fraction $\Omega_2$. It corresponds to the center of region II.

(iv) The final approach to saturation. The most favorably oriented domains grow at the expense of the less favorable ones. Gradually, the sample becomes a single domain with some lancet domains spread over its volume (region III in Fig. 1).

By decreasing the external field from the saturated state, the magnetization process follows the reverse order, and so on, successively. The field intensities where each of the above processes is active depend on the relative angle $\theta$ between the applied magnetic-field $H$ and the easy magnetic axis [001] and also on the size of the samples.[20,22] For these samples with $\theta° \leqslant \theta \leqslant 50°$, the major magnetization process is 180° wall motion.[20] The intensity of the applied magnetic field where there is the sudden growth of $\Omega_2$ is roughly proportional to $\theta$, as well as the volume fraction itself. The samples with $60° \leqslant \theta \leqslant 90°$ have larger volume fractions $\Omega_2$, even at $H=0$. On the other hand, the magnetic-field intensity required to produce the maximum of $\Omega_2$, is reduced as $\theta$ is increased from 60° to 90°.[20,22]

In the case of MI measurements, the magnetization distributions associated with these mechanisms may contribute, depending on the frequency of the ac field generated by the probe current, either with a DW or a rotational permeability, or both. Although DW motion is the main magnetization mechanism at low frequencies, it is strongly damped at frequencies above 1 kHz.[17] Thus, it is virtually absent in the range of frequencies used in this work, as discussed below.

### B. Connection to the MI features

All the above-described changes on domain structure are reflected in the effective transverse differential rotational permeability $\mu_{\text{eff}}$. Therefore, the distribution of the magnetization and its evolution are mapped in the MI behavior at different fields and frequencies.

For the low-frequency range ($f \leqslant 10$ kHz), the current is almost uniformly distributed over the sample's cross section. As a consequence, the MI probes $\mu_{\text{eff}}$ over the entire sample. As the frequency is increased, the current becomes restricted to the superficial skin layer defined by the skin-depth $\delta_m$. In view of that, the MI probes $\mu_{\text{eff}}$ from different parts of the domain structure: from the superficial closure (lancet or band) domains and from the main (striped or longitudinal) ones. When the volume fraction $\Omega_2$ of the lancet domain structure is strongly changed [step (ii) in the former description of the magnetization processes], a corresponding feature is expected to be present in the MI vs $H$ curves, *not associated with DW motion* but to the rotation of the magnetization as excited by the probe current. The field intensity and the details of these features will be different for each range of $\theta$, as follows.

#### 1. Small-angle range ($\theta \leqslant 20°$)

In this case, there are few modifications of the main domain structure, so the MI curves are smooth and have no modifications in shape as the frequency is increased. This behavior is exemplified in Fig. 3, for the $\theta=0°$ sample.

#### 2. Intermediate-angle range ($30° \leqslant \theta \leqslant 60°$)

In this range, the growth of the volume fraction occupied by the lancet domains ($\Omega_2$), corresponding to steps (ii) and (iii) of the magnetization process described in Sec. IV A, is larger than for the low-angle range. The contribution of this effect to $\mu_{\text{eff}}$ can be observed in Fig. 3, as the growth of the shoulder peaks at high fields (see the curves for the $\theta=50°$ sample). It should be also observed that these peaks are better seen at higher frequencies. This comes from the fact that the superficial domain structure has a greater contribution to $\mu_{\text{eff}}$ at increasing $f$, as expected from the skin effect.

#### 3. High-angle range ($70° \leqslant \theta \leqslant 90°$)

Here, the magnetization process has almost no 180° wall motion and stages (ii) and (iii) described in Sec. IV A, including the maximum in $\Omega_2$, happen at low applied magnetic fields. This feature will be responsible for the smoothness of the MI vs $H$ curves as seen in the corresponding panel of Fig. 3.

Thus, the MI vs $H$ curves can be connected to the features observed in the $M$ vs $H$ curves which, in turn, follow steps (i)–(vi) stated in Sec. IV A. In other words, the MI

measurements are useful to study complicated evolutions of domain structure, like these seen in (110)[001]$FeSi_{3\%}$.

### C. Rotation versus domain-wall motion

One point which has not been thoroughly taken care of in the above sections concerns the main contribution to the transverse differential permeability $\mu_{\text{eff}}(H,I_{\text{ac}},f)$, responsible for the observed MI effects. In the previous sections the rotational permeability was pointed out as the main contribution to $\mu_{\text{eff}}(H,I_{\text{ac}},f)$. In order to give a more substantial reason for such a statement, it is interesting to make a simple calculation of the impedance for a sample with the shape used in the present work. The exact calculation is intricate and should take into account the anisotropies in the differential permeability as well as complicated boundary conditions. The simplest but useful approximation is to consider the studied samples as infinite plates.[2] This approximation becomes reasonable when one considers that the ac current will be confined to a thin superficial layer due to the skin effect. The validity of this approximation rests on the comparison of its results to the experimentally obtained values for the differential permeability and skin depth at high frequencies.

Suppose initially that the plate surfaces are separated by a distance much larger than the skin depth, the samples can be approximated by a semi-infinite metal block. In this geometry the solution for the impedance is easily obtained as shown below.

For a semi-infinite metal block the current density ($J$) falls off from the surface as

$$J=J_0\ \exp\left[-(1+i)\ \frac{x}{\delta_m}\right], \tag{1}$$

where $J_0$ is the superficial current density, $x$ is a length measured from the surface toward the center of the cross section and $i=\sqrt{-1}$. The Ohmic losses at any point in a current-carrying conductor are given by $W=\rho|J|^2$ ($\text{W/m}^3$), where $\rho$ is the resistivity of the material. The eddy-current loss per square meter of cross-section surface is then given by

$$W=\int_0^\infty \rho|J|^2dx=\frac{\rho\,\delta_m}{2}\,|J_0|^2. \tag{2}$$

In this approximation, the loss per unit length for the $FeSi_{3\%}$ samples can be written as

$$|Z||I|^2=\frac{\rho|J_0|^2}{2}\ \delta_m 2w, \tag{3}$$

where $2w$ accounts for both skin layers active in each side of the sample. In the above expression $|Z|$ is the impedance per unit length. $|I|^2$ can be calculated from expression (1) as

$$|I|^2=2w^2\delta_m^2|J_0|^2. \tag{4}$$

Introducing expression (4) into expression (3) and normalizing by the dc resistance per unit length ($R_{\text{dc}}=\rho/wt$), the impedance can be expressed as

$$\frac{|Z|}{R_{\text{dc}}}=\frac{t}{2}\,\frac{1}{\delta_m}. \tag{5}$$

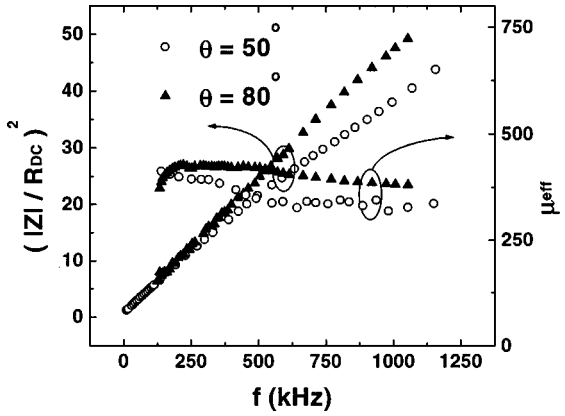


FIG. 6. $|Z/R_{\text{dc}}|^2\times f$ and $\mu_{\text{eff}}\times f$ plots for the $\theta=50°$ and 80°. Observe the roughly constant value attained by $\mu_{\text{eff}}$ at high frequencies.

Finally, introducing the expression for $\delta_m$ and squarying expression (5), one obtains:

$$\frac{|Z(H,f)|^2}{R_{\text{dc}}^2}=\frac{t^2}{2}\,\frac{\pi\mu_{\text{eff}}}{\rho}\,f. \tag{6}$$

A representative plot of $|Z(H,f)|^2/R_{\text{dc}}^2$ is shown in Fig. 6 for the $\theta=50°$ and $\theta=80°$ samples. In the same figure, the $\mu_{\text{eff}}$ vs $f$ curves obtained from expression (6) are also plotted. The values of $\mu_{\text{eff}}$ were about 420 and almost constant above about 150 kHz. These values are reasonable for bulk specimens which exhibit large losses at high frequencies like the $FeSi_{3\%}$ samples used in this work. The highest value obtained for the permeability corresponds to a skin depth of about 55 $\mu$m at 100 kHz (17 $\mu$m at 1 MHz). Both values characterize a strong skin regime.[9] The skin depth obtained for $f=1$ MHz and the observed $(Z/R_{\text{dc}})^2$ vs $f$ plots confirm that the initial approximation can be held above 30 kHz. These values also confirm that the MI experiments in these samples are probing the rotational response of the closure domain structure to the field generated by $I_{\text{ac}}$. For the $\theta=10°$ sample, however, the approximation fails because the sample is no longer in the strong skin regime, even for frequencies as high as 100 kHz. This fact is consistent with the behavior of the transverse differential permeability as a function of the angle $\theta$. The permeability first increases with $\theta$ up to $\theta\approx 60°$, decreasing for higher angles. Therefore, the range of frequencies where the semi-infinite block approximation is valid depends on the angle between the [001] axis and the direction of the current density.

From the comparison between the experimentally obtained data and the above calculations, it is reasonable to assume that for all samples studied in this work the dynamic magnetization process excited by the field associated with $I_{\text{ac}}$ is predominantly the rotation of the magnetization. So, the dc field $H$ changes the distribution of the magnetization [as described in steps (i)–(v), Sec. IV A], which in turn will change the transverse rotational differential permeability, as probed by MI measurements. Another feature which confirms the assumptions made at the beginning of the present calculation is the observed current independence of the MI. Also, as can be seen from Fig. 6, $\mu_{\text{eff}}\approx$constant over a wide frequency range. That means that just one magnetization pro-

cess is excited by the ac field, but it has contributions arising from the two domain families; the striped and closure ones.

## V. CONCLUSIONS

We have observed a very high magnetoimpedance effect in commercial $FeSi_{3\%}$ (110)[001]. By changing the angle between the applied magnetic field and the crystalline easy axis, both monotonic and nonmonotonic MI vs $H$ curves were obtained. The results can be understood in terms of basic magnetization processes in $FeSi_{3\%}$ combined with the skin-depth effect. The transverse differential permeability was shown to originate from spin rotation permeability, being roughly constant for frequencies up to 1 MHz. Values of the permeability were estimated from the $(Z/R_{dc})^2$ vs $f$ plots. It is shown that the MI measurements are a good complementary tool to study the magnetization processes in highly textured materials like the ones addressed in the present work.

## ACKNOWLEDGMENTS

This work is partially supported by CNPq, FAPERGS, and CAPES.

[1] L. D. Landau and E. M. Lifshitz, *The Electrodynamics of Continuous Media* (Pergamon, London, 1960).
[2] G. W. Carter, *The Electromagnetic Field in its Engineering Aspects* (Longmans, Green and Co., London, 1954).
[3] R. S. Beach and A. E. Berkowitz, Appl. Phys. Lett. **64**, 3652 (1994).
[4] L. V. Panina and K. Mohri, Appl. Phys. Lett. **65**, 1189 (1994).
[5] F. L. Machado, C. S. Martins, and S. M. Rezende, Phys. Rev. B **51**, 3926 (1995).
[6] L. V. Panina, K. Mohri, K. Bushida, and M. Noda, J. Appl. Phys. **76**, 6198 (1994).
[7] M. Knobel, M. L. Sánchez, A. Gómez-Polo, P. Marín, M. Vázquez, and A. Hernando, J. Appl. Phys. **79**, 1646 (1996).
[8] R. L. Sommer and C. L. Chien, Appl. Phys. Lett. **67**, 857 (1995).
[9] L. V. Panina, K. Mohri, T. Uchiyama, and M. Noda, IEEE Trans. Magn. **31**, 1249 (1995).
[10] R. L. Sommer and C. L. Chien, Appl. Phys. Lett. **67**, 3346 (1995).
[11] A. S. Antonov, S. N. Gadetskii, A. B. Granovskii, A. L. D'yachkov, V. P. Paramonov, N. S. Perov, A. F. Prokoshin, N. A. Usov, and A. N. Lagar'kov, Phys. Met. Metallogr. **83**, 612 (1997).
[12] J. Velásquez, M. Vázquez, D.-X. Chen, and A. Hernando, Phys. Rev. B **50**, 16 737 (1994).
[13] J. L. Costa-Krämer and K. V. Rao, IEEE Trans. Magn. **31**, 1261 (1995).
[14] M. Tejedor, B. Hernando, M. L. Sánchez, and A. García-Arribas, J. Magn. Magn. Mater. **157/158**, 141 (1996).
[15] M. Knobel, M. Vázquez, M. L. Sánchez, and A. Hernando, J. Magn. Magn. Mater. **169**, 89 (1997).
[16] M. Carara and R. L. Sommer, J. Appl. Phys. **81**, 4107 (1997).
[17] S. Chikazumi, *Physics of Magnetism* (Krieger, New York, 1978).
[18] G. Bertotti, F. Fiorillo, and M. P. Sassi, J. Magn. Magn. Mater. **23**, 136 (1981).
[19] M. Imamura and T. Sasaki, Phys. Scr. **24**, 29 (1988).
[20] R. L. Sommer and F. P. Livi, Phys. Status Solidi A **120**, 609 (1990).
[21] V. A. Zaykova, M. A. Vedenev, and V. K. Drozhzhina, Phys. Met. Metallogr. **35**, 32 (1973).
[22] P. Allia, A. Ferro-Milone, G. Montalenti, G. P. Soardo, and F. Vinai, IEEE Trans. Magn. **14**, 362 (1978).